IJMMM International Journal of Minerals, Metallurgy and Materials 矿物冶金与材料学报（英文版）

Microstructure and properties of a wear resistant Al–25Si–4Cu–1Mg coating prepared by supersonic plasma spraying

Tian-shun Dong, Ming Liu, Yang Feng, Guo-lu Li, and Xiao-bing Li

Cite this article as:
Tian-shun Dong, Ming Liu, Yang Feng, Guo-lu Li, and Xiao-bing Li, Microstructure and properties of a wear resistant Al–25Si–4Cu–1Mg coating prepared by supersonic plasma spraying, *Int. J. Miner. Metall. Mater.*, 27(2020), No. 9, pp. 1287-1294. https://doi.org/10.1007/s12613-019-1950-2

View the article online at SpringerLink or IJMMM Webpage.

International Journal of Minerals, Metallurgy and Materials
Volume 27, Number 9, September 2020, Page 1287
https://doi.org/10.1007/s12613-019-1950-2

Microstructure and properties of a wear resistant Al–25Si–4Cu–1Mg coating prepared by supersonic plasma spraying

Tian-shun Dong[1,2),*], *Ming Liu*[3)], *Yang Feng*[1),*], *Guo-lu Li*[1)], *and Xiao-bing Li*[1)]

1) School of Materials Science and Engineering, Hebei University of Technology, Tianjin 300130, China
2) Key Laboratory for New Type of Function Material in Hebei Province, Hebei University of Technology, Tianjin 300130, China
3) National Key Laboratory for Remanufacturing, Academy of Armored Forces Engineering, Beijing 100072, China
(Received: 26 October 2019; revised: 17 December 2019; accepted: 20 December 2019)

Abstract: A high content silicon aluminum alloy (Al–25Si–4Cu–1Mg) coating was prepared on a 2A12 aluminum alloy by supersonic plasma spraying. The morphology and microstructure of the coating were observed and analyzed. The hardness, elastic modulus, and bonding strength of the coating were measured. The wear resistance of the coating and 2A12 aluminum alloy was studied by friction and wear test. The results indicated that the coating was compact and the porosity was only 1.5%. The phase of the coating was mainly composed of α-Al and β-Si as well as some hard particles (Al_9Si, $Al_{3.21}Si_{0.47}$, and $CuAl_2$). The average microhardness of the coating was HV 242, which was greater than that of 2A12 aluminum alloy (HV 110). The wear resistance of the coating was superior to 2A12 aluminum alloy. The wear mechanism of the 2A12 aluminum alloy was primarily adhesive wear, while that of the coating was primarily abrasive wear. Therefore, it is possible to prepare a high content silicon aluminum alloy coating with good wear resistance on an aluminum alloy by supersonic plasma spraying.

Keywords: coating; high silicon aluminum alloy; microstructure; mechanical properties; wear resistance

1. Introduction

In recent years, high content silicon aluminum alloys have attracted to investigations into its performance (e.g., high specific strength, good thermal conductivity, and wear resistance) and potential applications [1–2]. Many countries have studied the production of engine cylinder liners with high content silicon aluminum alloys instead of cast iron, aiming to realize the manufacture of all-aluminum engine [3]. Currently, high content silicon aluminum alloys are mainly prepared using a spray forming technology [4–6]. The PEAK company of Germany has adopted a spray forming technology to produce a high content silicon aluminum alloy (Al–25Si–4Cu–1Mg) cylinder liner, which has been applied to Benz V6 and V8 engines. Nevertheless, a spray forming process has to be performed in a vacuum, it has many technological parameters, and it is a complicated operation. Additionally, there are too many defects produced by spray forming to meet the requirements of application. Therefore, hot extrusion treatment and heat treatment aging strengthening are needed to eliminate defects and improve mechanical properties, which makes the spray formed high content silicon aluminum alloy costly and inefficient [7].

We propose a solution for a high content silicon aluminum alloy suitable for some wear resistant components by coating of high silicon aluminum alloy on the surface of an aluminum alloy with certain strength using thermal spray technology. Thermal spraying technology has some advantages, such as it requires simple equipment, convenient operation, and low cost [8–9], hence, this solution is of great significance to efficiency and economy. However, there have been no reports on the preparation of high silicon aluminum alloy coatings with a thermal spray technology [10].

An Al–25Si–4Cu–1Mg coating was prepared by supersonic plasma spraying, and the structure, mechanical properties, and wear resistance of the coating were studied. The feasibility of preparing a high content silicon aluminum alloy coating by supersonic plasma spraying was explored.

2. Experimental

The powder size was 15–45 μm and its morphology is

*These authors contributed equally to this work.
Corresponding authors: Ming Liu E-mail: hzaam@163.com; Guo-lu Li E-mail: liguolu0305@163.com

shown in Fig.1. The chemical composition of powder was 25wt% Si, 4wt% Cu, 1wt% Mg, and remaining Al. When Mg and Cu elements were added to the high content silicon aluminum alloy, they can form strengthening phase of Mg_2Si and $CuAl_2$ respectively, thus improve the mechanical properties and wear resistance of the alloy [11]. The substrate was a common high strength aluminum alloy, 2A12, and the size was 60 mm × 12 mm × 5 mm. The chemical composition of the substrate was 3.8wt%–4.9wt% Cu, 1.2wt%–1.8wt% Mg, 0.3wt%–0.9wt% Mn, and remaining Al.

The spraying equipment was a high efficiency supersonic plasma spraying system (HEPJet) and the spraying parameters are shown in Table 1. Before spraying, the substrate was cleaned by an ultrasonic wave in acetone and then sand blasted. During the spraying, the substrate was cooled by high pressure air behind the plate substrate to prevent the substrate from overheating. The coating thickness was 500 μm.

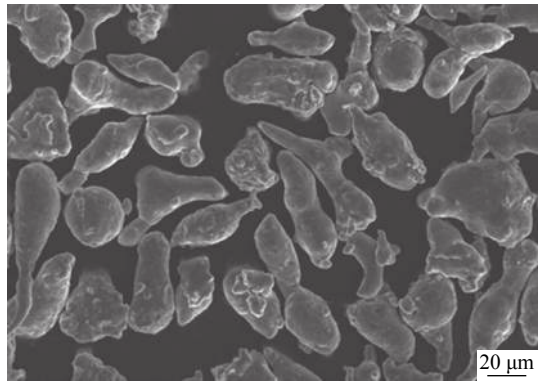

Fig. 1. Morphology of the spray powder.

Table 1. Main parameters of the supersonic plasma spraying

Current / A	Voltage / V	Primary gas flow (Ar) / ($L \cdot min^{-1}$)	Secondary gas flow (H_2) / ($L \cdot min^{-1}$)	Spray distance / mm	Powder feed / ($g \cdot min^{-1}$)	Gun travel distance / ($mm \cdot s^{-1}$)
330	120	120	10.8	100	30	67

The wear properties of the coating were tested by a CETR UMT-3 friction and wear tester. The diameter of the grinding ball was 4 mm, the material was GCr15, the frequency was 2 Hz, the reciprocating distance was 4 mm, the wear time was 30 min, and the load was 2 N. The morphology of the coating, wear marks, and debris were observed and analyzed by scanning electron microscopy (SEM, FEI Nova NanoSEM50) and an energy dispersive spectrometer (EDS, Oxford X-Max 80). The phase of the coating and powder were measured by X-ray diffraction (XRD, Bruker D8 ADVANCE), and the scanning speed was 4°/min and the diffraction angle was 20°–90°. The microhardness of the coating was tested by a Buehler Micromet-6030 microhardness tester. The load was 100 g and the loading time was 20 s. The elastic modulus of the coating was measured by a MTS Nano Indenter XP nanoindentation tester. The bonding strength of the coating was tested according to ASTM C633. The tensile test of the coating was performed on a MTS809 high temperature electronic universal material testing machine and average value of four experiments were used. The microstructure and phase composition of the coating were analyzed by transmission electron microscopy (TEM, FEI Tecnai G2 F20). The wear volume and wear width of the coating were measured by a LEXT OLS4000 3D laser measuring microscope.

3. Results and discussion

3.1. Morphology of coating

The surface morphology of the Al–25Si–4Cu–1Mg coating is shown in Fig. 2(a). The surface of the coating was rough, and there were some defects such as unmelted particles and pores on the surface. The cross-sectional morphology of the coating is shown in Fig. 2(b). The porosity of the coating measured by image grayscale analysis method was only 1.5%, as shown in Fig. 2(c), but that of the spray formed high silicon aluminum alloy was 2%–5% [12]. Owing to the proper process parameters, the coating was very uniform and compact. The pores and unmelted particles were fewer because the flight speed of the droplets in the supersonic plasma spraying was faster than that in the conventional plasma spraying, the kinetic energy of droplets was larger. When droplets impacted the substrate, they were easier to spread, hence the coating was compact. Moreover, the melting point of the aluminum alloy was low, while the flame temperature of the supersonic plasma spraying was high, so it was difficult to form unmelted particles.

3.2. Microstructure of the coating

An important factor to evaluate the quality of a high silicon aluminum alloy was the size and morphology of the β-Si phase. The coarse and stripped β-Si phase was easy to break and fracture when the alloy was loaded, which reduced the plasticity, toughness, and wear resistance of the alloy [13–14]. The cross-sectional morphology of the coating after corrosion is shown in Fig. 3. As shown in Fig. 3(a), the structure of the coating mainly consists of the α-Al matrix and the β-Si hard phase (α-Al is the solid solution of Si in Al and β-Si is the solid solution of Al in Si). The β-Si phase is uniformly distributed on the α-Al matrix, its shape is a regular block, and the size was 2–5 μm. The size of the β-Si phase in spray formed high content silicon aluminum alloy was 5–30 μm,

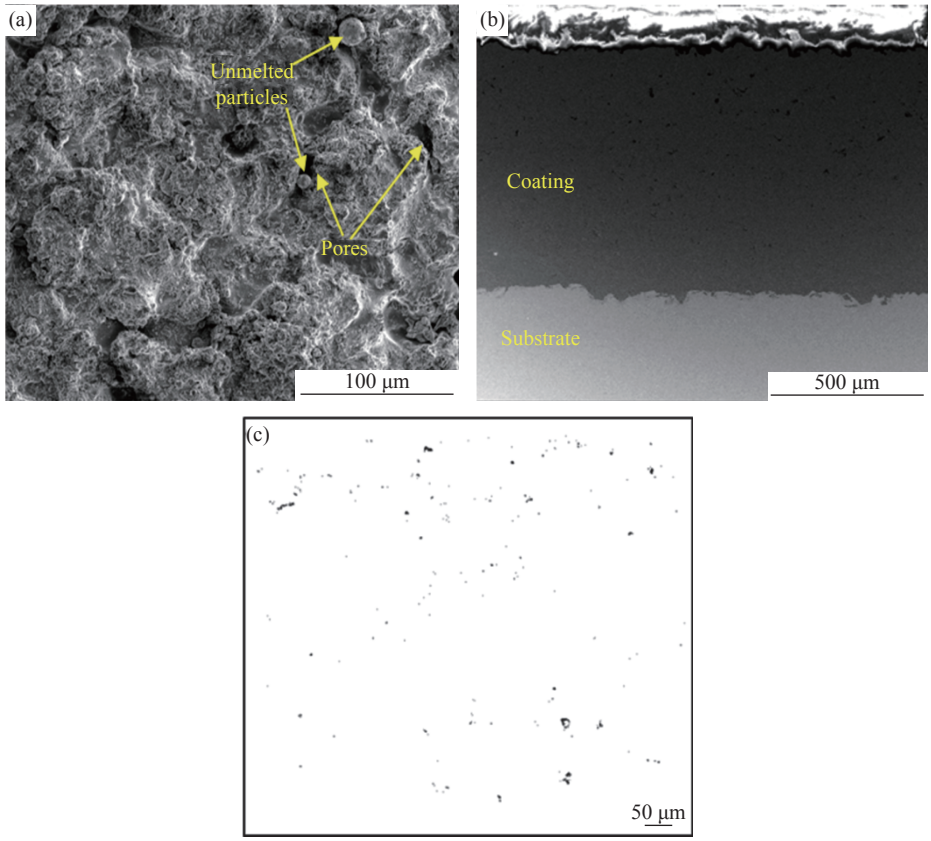

Fig. 2. Morphology of the coating: (a) surface; (b) cross section; (c) gray image of cross section.

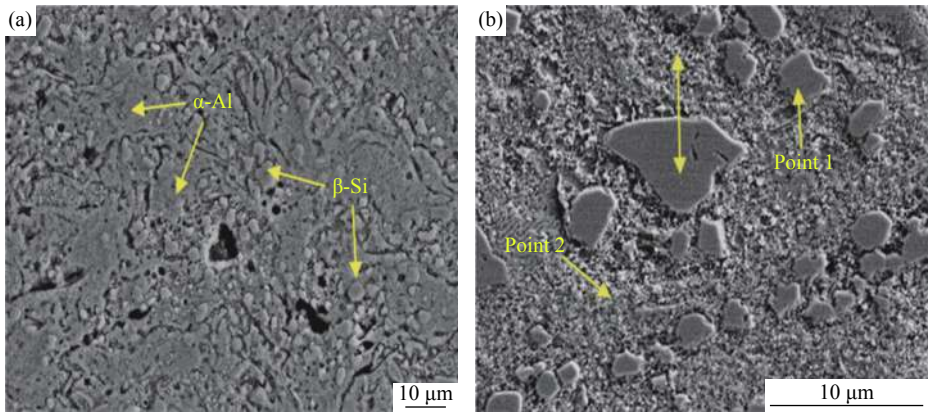

Fig. 3. Morphology of the coating after corrosion: (a) cross-sectional morphology; (b) larger image.

and the size was not uniform and mostly striped [15].

The cause of the different β-Si phases was that during spray forming, the metal droplets was larger and not uniform (15–200 μm). For spraying, the powder with size of 15–45 μm was heated into droplets and then sprayed onto the surface of the substrate. Therefore, the initial size of the droplets was limited to 45 μm. When high-speed droplets impacted the substrate, they would spread out instantaneously. Moreover, the use of a cooling device controlled the substrate to below 100°C during the spraying process. Hence, the cooling speed of the droplets was faster than that of the spray formation. When the droplets impacted the substrate, they solidified instantaneously, thus the precipitation and growth of the β-Si phase was inhibited.

In addition, as shown in Fig. 3(b), β-Si was well bonded with α-Al. The EDS analyses of points 1 and 2 were shown in Table 2. The content of Si in α-Al reached 13.82wt%. As the solid-solved Si in α-Al cannot be completely precipitated from α-Al during the cooling process, α-Al formed a supersaturated solid solution. Si then plays a role in solid solution strengthening, leading to an increase in the hardness of the coating. The EDS analysis of the interface between α-Al and

β-Si in Fig. 3(b) is shown in Fig. 4. The Al and Si elements gradually changed at the interface between α-Al and β-Si, and there was no abrupt change in the content at the interface, which was beneficial to the bonding strength of the α-Al and β-Si.

Table 2. EDS analyses of points 1 and 2 in Fig. 3(b) wt%

Point number	Al	Si	Cu	Mg
No. 1	0.15	97.99	1.40	0.46
No. 2	80.97	13.82	4.12	1.09

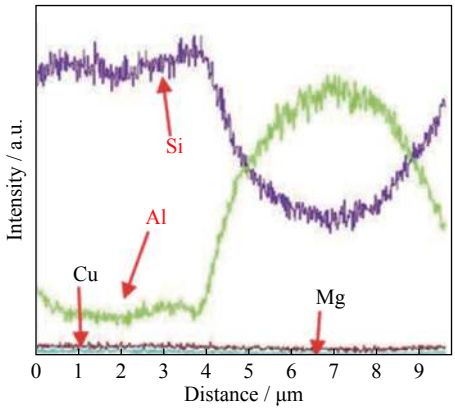

Fig. 4. EDS analysis of the interface.

3.3. Phase of the coating

The XRD analysis of the coating and powder are shown in Fig. 5. The phase composition of the coating was consistent with the powder, which was mainly comprised of α-Al, Al_9Si, $Al_{3.21}Si_{0.47}$, β-Si, and $CuAl_2$ phases. No oxides were detected in the coating, indicating that Ar gas effectively isolated the air during the spraying process and prevented the droplets from being oxidized. The secondary gas in spraying was H_2, which belonged to reduction gas for most metals. Hence, adding H_2 could partially prevent the oxidation of materials.

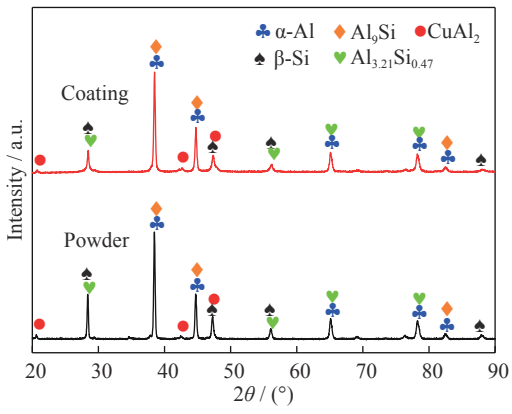

Fig. 5. XRD patterns of the coating and powder.

In addition, Fig. 5 shows the peak strength of the β-Si phase in the coating was less than that of the powder because the powder was heated to the melting state by spraying and the β-Si phase in the powder was melted. When the droplets impacted the substrate, the cooling rate of the droplets was large and it is difficult for the β-Si phase to sufficiently precipitate. As a result, the β-Si phase in the coating was less than that in the powder. Nevertheless, the content of Si dissolved in α-Al was high, which can play a role in the solid solution strengthening. This was confirmed by Table 2.

The TEM image of the coating is shown in Fig. 6. As shown in Fig. 6(a), the coating was mainly divided into two regions, i.e., A and B. The A region was a single crystal region and its diffraction pattern is shown in the upper left corner of Fig. 6(a). The EDS analysis in Fig. 6(b) reveals that the main components of the A region were Al and Si elements. Combined with the analysis of the microstructure and XRD of the coating, the A region should be the β-Si phase. The diffraction pattern of the B region is shown in the lower right corner of Fig. 6(a), which consists of a diffraction spot and diffraction ring, indicating that the B region is a mixed crystal region. It can be inferred that the B region was α-Al. The magnified image of the B region and its EDS analysis is shown in Fig. 6(b). Some nanometer and submicron $CuAl_2$, Al_9Si, and Si particles were distributed evenly on α-Al matrix. Fig. 6(c) is a magnified image of the interface between the A and B regions. There were no cracks or other impurities at the interface, indicating that β-Si and α-Al had excellent combination. In summary, the structure of the coating was as follows: some large β-Si phases and fine discrete $CuAl_2$, Al_9Si, and Si particles distributed evenly on α-Al matrix, and these strengthening phases were closely bound to the α-Al matrix.

3.4. Mechanical properties of the coating

The microhardness of the cross section of the coating is shown in Fig. 7. The average microhardness of the coating reached HV 242. The fluctuation of microhardness from the surface to the bottom was not large, and the lowest hardness was HV 212, which was significantly greater than that of the 2A12 aluminum alloy after heat treatment (HV 110 [12]) and the spray formed high content silicon aluminum alloy (about HV 145 [5–6]). The higher hardness of the coating can be attributed to three reasons. First, the spraying coating was more compact than the spray formed components. Second, the β-Si phase in the spraying coating was finer and more dispersed, playing a role in the dispersion strengthening. Finally, Si dissolved in the α-Al matrix was supersaturated, playing a role in the solution strengthening. Therefore, the hardness of the coating was greater.

The elastic modulus and bonding strength of the coating are shown in Table 3. The average bonding strength of the coating was 46 MPa. The elastic modulus of the coating was

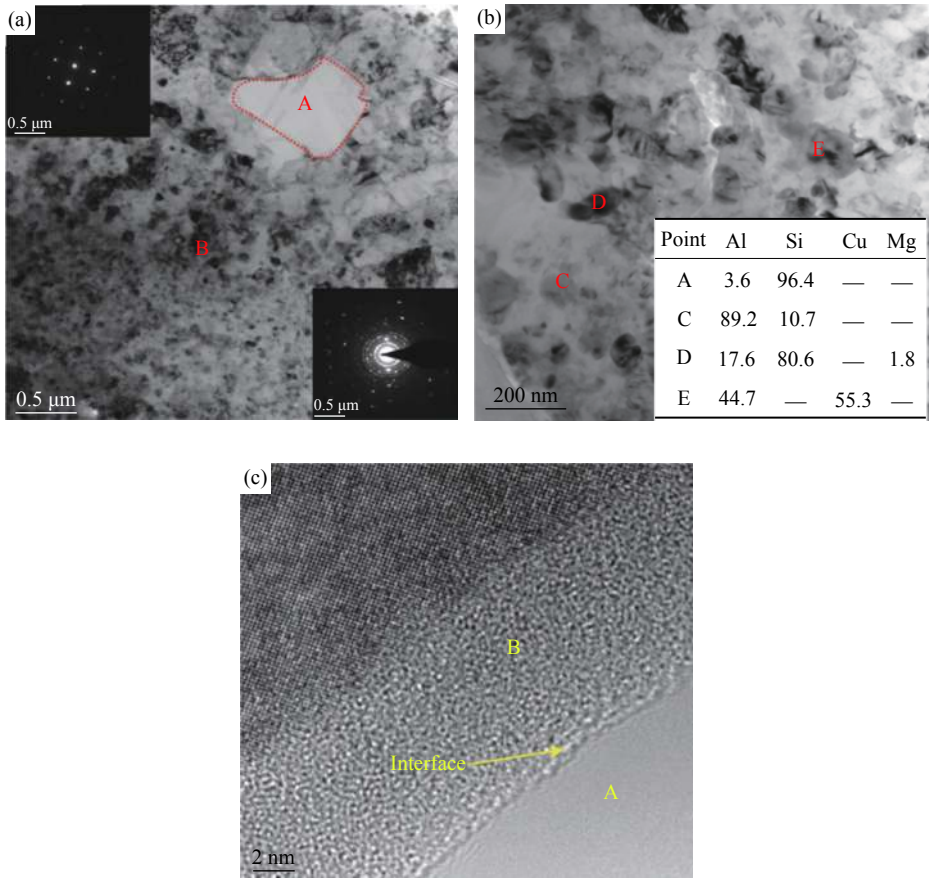

Fig. 6. TEM morphology and EDS analysis (wt%) of the coating: (a) coating; (b) magnified image of the B region;(c) magnified image of the interface between the A and B regions.

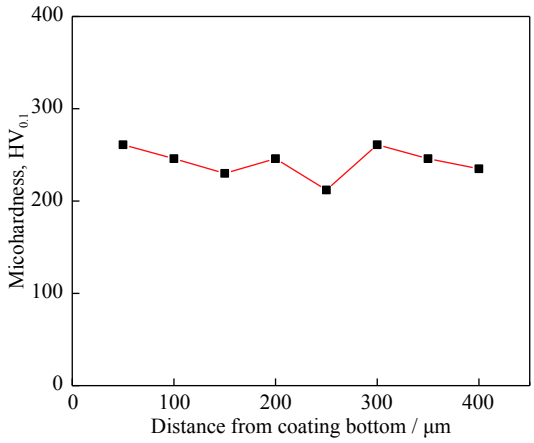

Fig. 7. Microhardness curve of the coating.

about 75.7 GPa, which was very close to that of the 2A12 aluminum alloy (73 GPa). The smaller the difference of the elastic modulus between the coating and the substrate was, the less significant the stress was generated at the interface during loading, which was beneficial to the bonding strength of the coating.

Table 3. Mechanical properties of the coating

Elastic modulus / GPa	Bonding strength / MPa
75.7 ± 6	46 ± 3

3.5. Wear resistance of coating

The coefficient of friction (COF) of the 2A12 aluminum alloy and Al–25Si–4Cu–1Mg coating are shown in Fig. 8. The aluminum alloy had obvious running in the stage from 0

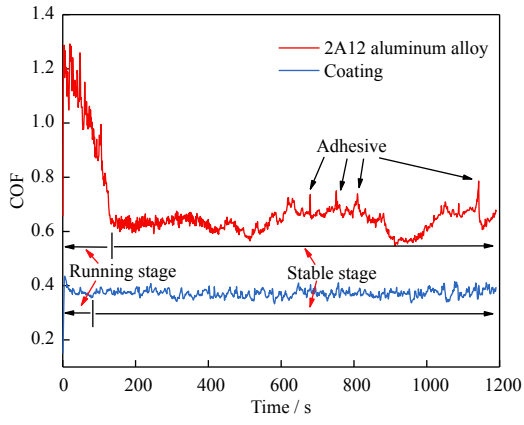

Fig. 8. COF of the 2A12 aluminum alloy and coating.

to 150 s, and its COF was large at the beginning because the aluminum alloy was very soft. When the load was applied to the grinding ball, the grinding ball would be pressed into the aluminum alloy. Consequently, the resistance to the grinding ball plowing the aluminum alloy was larger, resulting in a greater COF in the running in stage. However, as the aluminum alloy was gradually plowed, the resistance decreases, leading to the COF gradually decreasing. In the stable wear stage, the COF of the aluminum alloy fluctuated about 0.6, and the fluctuation range was large (about 0.2). The COF suddenly increased at some points, indicating adhesive wear on the surface of the aluminum alloy.

In comparison, the COF of the coating was relatively stable from the beginning to the end of the wear test. There was nearly no obvious running in the stage. This is because the hardness of the coating was greater, the grinding ball was pressed into the coating shallowly, and the resistance to the grinding ball was small when the coating was furrowed, leading to a smaller COF of the coating at the beginning of the wear test. The COF of the coating in the stable wear stage fluctuated around 0.4, which was less than that of the aluminum alloy. Moreover, the fluctuation range was very small (less than 0.06), demonstrating nearly no adhesion occurred in the sprayed coating, and the wear resistance of the coating surface and coating interior were uniform and consistent.

The wear scar width and volume of the aluminum alloy and coating measured by the 3D (three dimensional) laser measuring microscope are shown in Fig. 9. As the grinding ball was a steel ball with diameter of 4 mm, the deeper the grinding ball was pressed into the sample, the wider the wear scar width. Therefore, the wear scar width reflects the wear scar depth and the wear volume. The wear scar width of the aluminum alloy was 1202 μm, while that of the coating was only 481 μm, 2.5 times less than the alloy. The wear scar volume of the aluminum alloy was 5.56×10^{-2} mm^3, while that of the coating was only 1.56×10^{-2} mm^3, 3.6 times less than the alloy. Therefore, the wear resistance of the Al–25Si–4Cu–1Mg coating was significantly superior to the 2A12 aluminum alloy.

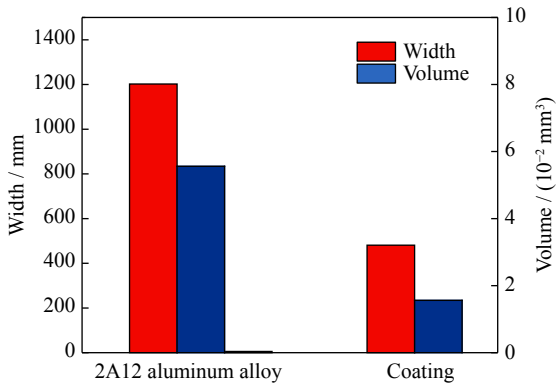

Fig. 9. Wear width and volume of the 2A12 aluminum alloy and coating.

The wear scar morphology was observed to analyze the wear mechanism. The wear scar morphology of the aluminum alloy in Fig. 10(a) indicates obvious plows on the surface of the wear scar with a large number of debris adhered. This demonstrates that the wear mechanism of the aluminum alloy includes adhesive and abrasive wear, and the main wear mode was adhesive wear. Fig. 10(b) reveals that the debris of the aluminum alloy was flaky. The aluminum alloy possessed relatively low strength and was prone to plastic deformation and adhesion, the debris fell off, and the surface was rolled into a flat shape during the reciprocating sliding process.

The wear scars of the coating are shown in Fig. 10(c). There were many plows on the surface with fine abrasive debris adhered to them. However, the plows of the coating were shallower than that of the aluminum alloy, and the size of the abrasive debris was smaller. Fig. 10(d) shows that the wear debris of the coating was granular. These images indicate that the wear mechanism of the coating was abrasive wear and adhesive wear, but its wear degree was much less than that of the aluminum alloy, and the main wear mode was abrasive wear.

The reason for the good wear resistance of the coating is described below.

The average hardness of coating was HV 242, while the 2A12 aluminum alloy was only HV 110. According to the abrasive wear model proposed by Rabinowicz [16], the mathematical expression of the wear volume V was as follows:

$$V = K\frac{LP}{H} \tag{1}$$

where K was the wear factor, L was the distance of the sliding, P was the applied load, and H was the hardness of the material. As shown in Eq. (1), the abrasive wear volume V was inversely proportional to the hardness of the material, so the abrasive wear of the coating was relatively slight. According to the theory of the adhesion wear proposed by Archard, the wear volume was also inversely proportional to the hardness of the material so the adhesion wear of the coating was also relatively slight [17]. In addition, the Al–25Si–4Cu–1Mg coating was mainly composed of an α-Al matrix and dispersed hard phases (β-Si, Al_9Si, $Al_{3.21}Si_{0.47}$, and $CuAl_2$). These hard phases could resist the plowing of the grinding ball and debris during friction, and reduce the contact area between α-Al matrix and grinding ball, thereby reducing adhesion. Even if the β-Si would break and peel off during wear, some of the fine abrasives could prevent the adhesion between the grinding ball and the coating, and play a role in the antifriction, thereby reducing the COF [18]. Therefore, the wear resistance of the coating was superior to the 2A12 aluminum alloy.

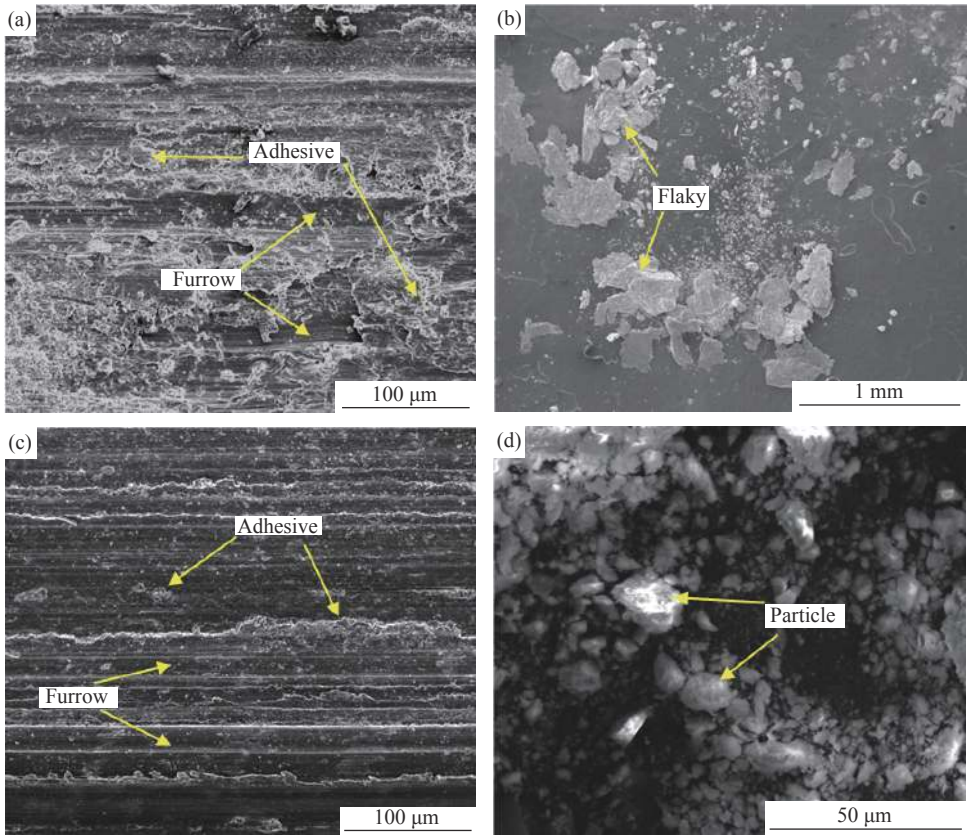

Fig. 10. Wear marks and debris morphology of the (a, b) 2A12 aluminum alloy and (c, d) coating.

4. Conclusions

An Al–25Si–4Cu–1Mg coating was prepared on a 2A12 aluminum alloy by supersonic plasma spraying, and the resulting structure, mechanical properties, and wear resistance of the coating were studied. The conclusions are as follows.

(1) The porosity of the coating was only 1.5%. The phase of the coating was mainly composed of α-Al and β-Si, as well as Al_9Si, $Al_{3.21}Si_{0.47}$, and $CuAl_2$. The Si particles were small (2–5 μm), dispersed, and bound closely with α-Al to strengthen the coating.

(2) The average microhardness of the coating was HV 242, which was remarkably higher than those of the 2A12 aluminum alloy (HV 110) and spray formed high silicon aluminum alloy (about HV 145). The bonding strength between the coating and substrate was about 46 MPa.

(3) The wear resistance of the Al–25Si–4Cu–1Mg alloy coating was significantly superior to the 2A12 aluminum alloy. The main wear mechanism of the 2A12 aluminum alloy was adhesive wear, while that of the Al–25Si–4Cu–1Mg alloy coating was abrasive wear.

Therefore, it is feasible to prepare a high content silicon aluminum alloy coating with good wear resistance by supersonic plasma spraying.

Acknowledgements

This work was financially supported by the National Natural Science Foundation of China (Nos. 51675158, 51535011, and 51675531), the Natural Science Foundation of Hebei Province (No. E2016202325), and the Beijing Municipal Natural Science Foundation (No. 3172038).

References

[1] L.G. Hou, C.L. Cui, and J.S. Zhang, Optimizing microstructures of hypereutectic Al–Si alloys with high Fe content via spray forming technique, *Mater. Sci. Eng. A*, 527(2010), No. 23, p. 6400.

[2] F.M. Du, C.D. Li, Z.T. Mi, Y. Shen, R.X. Huang, X.G. Han, Y. Dong, and J.J. Xu, Anti-wear property of aluminum–silicon alloy treated by chemical etching, mechanical honing and laser finishing, *Materials*, 12(2019), No. 8, p. 1273.

[3] D. Lawrynowicz, X. Liang, T.S. Srivatsan, and E.J. Lavernia, Processing, microstructure and fracture behaviour of a spray-atomized and deposited nickel aluminide intermetallic, *J. Mater. Sci.*, 33(1998), No. 6, p. 1661.

[4] Y.G. Chen, H. Yang, B.Q. Zhang, Y.L. Liu, J.C. Yin, W. Wei, and Y. Zhong, A novel restraint spraying-conform process for manufacturing hypereutectic Al–Si alloy with enhanced properties, *Mater. Res. Express*, 4(2017), No. 2, art. No. 026502.

[5] L.G. Hou, Y.H. Cai, H. Cui, and J.S. Zhang, Microstructure

evolution and phase transformation of traditional cast and spray-formed hypereutectic aluminium–silicon alloys induced by heat treatment, *Int. J. Miner. Metall. Mater.*, 17(2010), No. 3, p. 297.

[6] Y.S. Niu, J.C. Yin, Y.L. Liu, B.Q. Zhang, Y.F. Li, Y.G. Chen, and Y. Zhong, Microstructure, mechanical properties and wear behaviour of Al–20Si–3Fe alloy prepared by spray Conform, *Mater. Res. Express*, 6(2019), No. 8, art. No. 086578.

[7] Z.Y. Cai, C. Zhang, R.C. Wang, C.Q. Peng, K. Qiu, and Y. Feng, Preparation of Al–Si alloys by a rapid solidification and powder metallurgy route, *Mater. Des.*, 87(2015), p. 996.

[8] M.L. Dong, X.F. Cui, B.W. Lu, X.R. Feng, G. Jin, L. Shi, and H.D. Wang, Accelerated diffusion of carbon and grain refinement of vacuum carburized layer by La ion implantation, *J. Alloys Compd.*, 814(2020), art. No. 152308.

[9] J. Su, J.J. Kang, W. Yue, G.Z. Ma, Z.Q. Fu, L.N. Zhu, D.S. She, H.D. Wang, and C.B. Wang, Comparison of tribological behavior of Fe-based metallic glass coatings fabricated by cold spraying and high velocity air fuel spraying, *J. Non-Cryst. Solids*, 522(2019), p. 119582.

[10] Z.Y. Piao, B.S Xu, H.D Wang, and X.X. Yu, Rolling contact fatigue behavior of thermal-sprayed coating: A review, *Crit. Rev. Solid State Mater. Sci.* (2019). DOI: 10.1080/10408436.2019.1671798

[11] C.M. Chen, C.C. Yang, and C.G. Chao, A novel method for net-shape forming of hypereutectic Al–Si alloys by thixocasting with powder preforms, *J. Mater. Process. Technol.*, 167(2005), No. 1, p. 103.

[12] J.F. Zhao and X.G. Yuan, Densification of spray-formed Al–22%Si alloy, *J. Mudanjiang Univ.*, 26(2017), No. 11, p. 148.

[13] Y.D. Jia, F.Y. Cao, P. Ma, S. Scudino. J. Eckert, J.F. Sun, and G. Wang, Microstructure and thermal conductivity of hypereutectic Al-high Si produced by casting and spray deposition, *J. Mater. Res.*, 31(2016), No. 19, p. 2948.

[14] F. Wang, Y.J. Ma, Z.Y. Zhang, X.H. Cui, and Y.S. Jin, A comparison of the sliding wear behavior of a hypereutectic Al–Si alloy prepared by spray-deposition and conventional casting methods, *Wear*, 256(2004), No. 3-4, p. 342.

[15] F.L. Yang, W. Zhang, D.Q. Yi, R.C. Wang, and Z.K. Chen, Microstructure analysis of rapidly solidified Al–40Si alloy fabricated by spray deposition, *Powder Metall. Technol.*, 24(2006), No. 3, p. 166.

[16] E. Rabinowicz, *Friction and Wear of Materials*, John Wiley & Sons, Inc., New York, 1965.

[17] L. Frérot, R. Aghrotababaei, and J.F. Molinari, A mechanistic understanding of the wear coefficient: From single to multiple asperities contact, *J. Mech. Phys. Solids*, 114(2018), p. 172.

[18] H.L. Si, *Study on Heat Treatment and Wear Resistance of Spray Formed High Silicon Aluminum Alloy* [Dissertation], Harbin University of Science and Technology, Harbin, 2008.